JOURNAL OF GEOPHYSICAL RESEARCH, VOL. 105, NO. B6, PAGES 13,595–13,612, JUNE 10, 2000

An induced seismicity experiment across a creeping segment of the Philippine Fault

R. Prioul,[1] F.H. Cornet,[1] C. Dorbath,[2] L. Dorbath,[2]
M. Ogena,[3] and E. Ramos[4]

Abstract. The location of seismicity induced by forced fluid flow provides information about domains of pore pressure variation, while changes in fluid content are identified through changes in seismic velocity. These effects have been investigated in the geothermal field of Tongonan, which lies on a creeping portion of the Philippine Fault on Leyte Island. Locally, the left-lateral strike-slip Philippine Fault branches out into three subparallel segments (Eastern, Central and Western Fault Lines). In June-July 1997, a water stimulation was undertaken in a well that intersects the Central Fault Line 1980 m below ground surface; 36,000 m^3 were injected between the casing shoe at 1308 m and the well bottom at 2177 m. The seismicity was monitored with a surface station network of 18 stations. More than 400 events, induced by the injection experiment as well as by routine injections associated with the geothermal field exploitation, were recorded in the vicinity of the well. They have been located through a simultaneous three-dimensional (3-D) velocity-hypocenter inversion procedure. None of the microearthquakes are located along the Central Fault Line, they all occurred below the casing shoe to the east of the fault line, i.e., within the geothermal reservoir and mostly below the bottom of the well. Results from the injection experiment and the 18 months of seismic monitoring along the Central and West Fault Lines suggest an aseismic behavior of this major continental fault at this location. The 3-D velocity model, determined from the travel time inversion for seismic events observed during injections, is compared to that obtained from seismic monitoring conducted prior to any injection activities. An increase of P wave velocity is observed during the water injection. This velocity increase is localized within the seismicity cloud and is interpreted as an increase in liquid content within the initial liquid-vapor multiphase part of the reservoir.

1. Introduction

In June 1997, a large water injection experiment was undertaken across a segment of the Philippine Fault on Leyte Island, at the Tongonan geothermal field (Figures 1a and 1b). The Philippine Fault is a major left-lateral strike-slip fault located behind a subduction zone. It extends over 1200 km through the whole Philippine archipelago [*Allen*, 1962; *Fitch*, 1972; *Barrier et al.*, 1990]. Geological observations and kinematic analysis yield a shear displacement rate of 2 to 2.5 cm yr^{-1} for the fault [*Barrier et al.*, 1991]. Repeated Global Positioning System (GPS) measurements conducted in between 1991 and 1995 have shown that the fault creeps at a rate of 3.5 cm yr^{-1} [*Duquesnoy*, 1997] on the northern Leyte segment of the Philippine Fault (11°05′-11°30′N). The geothermal field is located where the fault intersects a volcanic arc (Figure 1b). On site, the fault zone is divided into three main parallel vertical segments (at least down to 2.5 km, as shown by seismic profiles); they are referred to the Eastern, Central, and Western Fault Lines (Figure 1c). Six GPS campaigns conducted across the West and Central Fault Lines between 1991 and 1997 have shown that locally the fault creeps at a rate of 2.4 cm yr^{-1} [*Duquesnoy et al.*, 1994; *Duquesnoy*, 1997; *Bacolcol*, 1999]. Although no large historical seismic event has been observed in the northern part of the island (11°05′-11°30′N), one event with magnitude 5.4 occurred on May 17, 1993, in the vicinity of the central section of the fault (Figure 1b). A

[1]Département de Sismologie, Institut de Physique du Globe de Paris, France.
[2]Département de Sismologie, Institut de Physique du Globe de Strasbourg, France.
[3]Philippine National Oil Company, Energy Development Corporation, Makati City, Philippines.
[4]Philippine Institute of Volcanology and Seismology, Quezon City, Philippines.

Copyright 2000 by the American Geophysical Union.

Paper number 2000JB900052.
0148-0227/00/2000JB900052$09.00

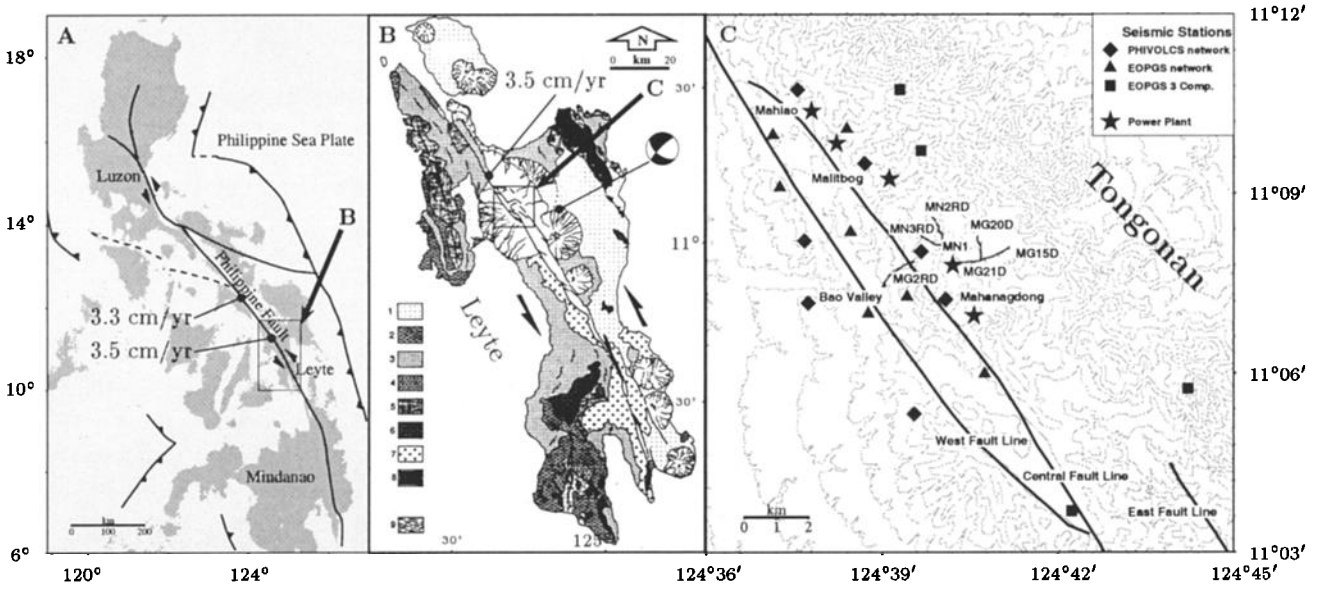


Figure 1. (a) The major left-lateral strike-slip Philippine Fault is located behind a subduction zone and extends over 1200 km through the whole Philippine archipelago. Repeated GPS measurements yield a shear displacement rate of 3.5 cm yr^{-1} on the northern Leyte 50 km segment and close to 3.3 cm yr^{-1} on the Masbate Island segment (measurements from *Duquesnoy* [1997]). (b) Structural map of Leyte Island where the fault intersects a volcanic arc (modified from *Aurelio* [1992], 1, recents volcanics; 2 and 4, Pleistocene and mid-Miocene limestones; 3 and 5, late and mid-Miocene sediments; 6, volcanoclastics; 7, magmatic rocks; 8, ophiolits; 9, marine deposits). The only known earthquake in central Leyte larger than magnitude 5 is also displayed. (c) Map of the Tongonan geothermal site where the fault zone is divided into three main parallel segments, called the Eastern, Central, and Western Fault Lines. Locations of the 18 seismic stations are displayed as well as the horizontal projection of well MG2RD and the power plants. Single and three component stations from PHIVOLCS and EOPGS Instituts have been used (see text for details). Topographic contour lines are displayed every 100 m.

few moderate events with magnitude close to 6 have occurred since 1980 in the southern section (10°-10°30′N).

For the last 10 years, the Tongonan geothermal field has been extensively developed, and large amounts of brines, generated by the exploitation, have to be reinjected. For that purpose, a few boreholes were drilled in between the Western and Eastern Fault Lines. These were found to be impervious. One of these wells was selected to conduct a hydraulic stimulation experiment. A characteristic of the selected nonvertical well is that it intersects one branch of the central fault. The concept of the experiment was to slowly build up the injection flow rate so as to stimulate, by shearing and cooling, the preexisting fractures intersected by the well [*Cornet and Jones,* 1994; *Cornet et al.,* 1997]. Prior to this injection a surface seismic network was installed in order to monitor any induced seismic activity.

After a short description of the injection experiment and of the seismic monitoring system, this paper presents the results of the induced seismicity analysis. Local earthquake travel times recorded during the experiment period are inverted in order to simultaneously obtain the three-dimensional (3-D) velocity structure and the location of hypocenters. Precise relocations of seismic events are analyzed in terms of domains of pore pressure variation in the vicinity of the fault. Results of the 3-D velocity structure variation with time are discussed in terms of fluid content changes and temperature perturbations caused by injections. Finally, a mechanism for interpreting the observed seismicity is discussed.

2. Injection Experiment

A large hydraulic injection experiment has been undertaken in well MG2RD (Figures 1c and 2). This deviated well was selected because it intersects the Central Fault Line ~1980 m below ground surface according to geological interpretation (Figure 3; depths are hereinafter referred as meters below ground surface: m bgs). The intersection with the fault was confirmed by a thermal discontinuity, observed on a thermal log conducted just after drilling (Figure 4). The wellhead is located 260 m above sea level, while the bottom of the well is located 2177 m bgs to the east of the fault [*Bondocoy,* 1993]. The borehole is cased down to a depth of 1308 m bgs. Below this depth, the slotted liner section (perforated pipe allowing inward and outward flow) intersects the Mahanagdong Claystone (MC) and then penetrates the Mahiao Sedimentary Complex (MSC) after it has crossed the central fault. The Mahanagdong Clay-

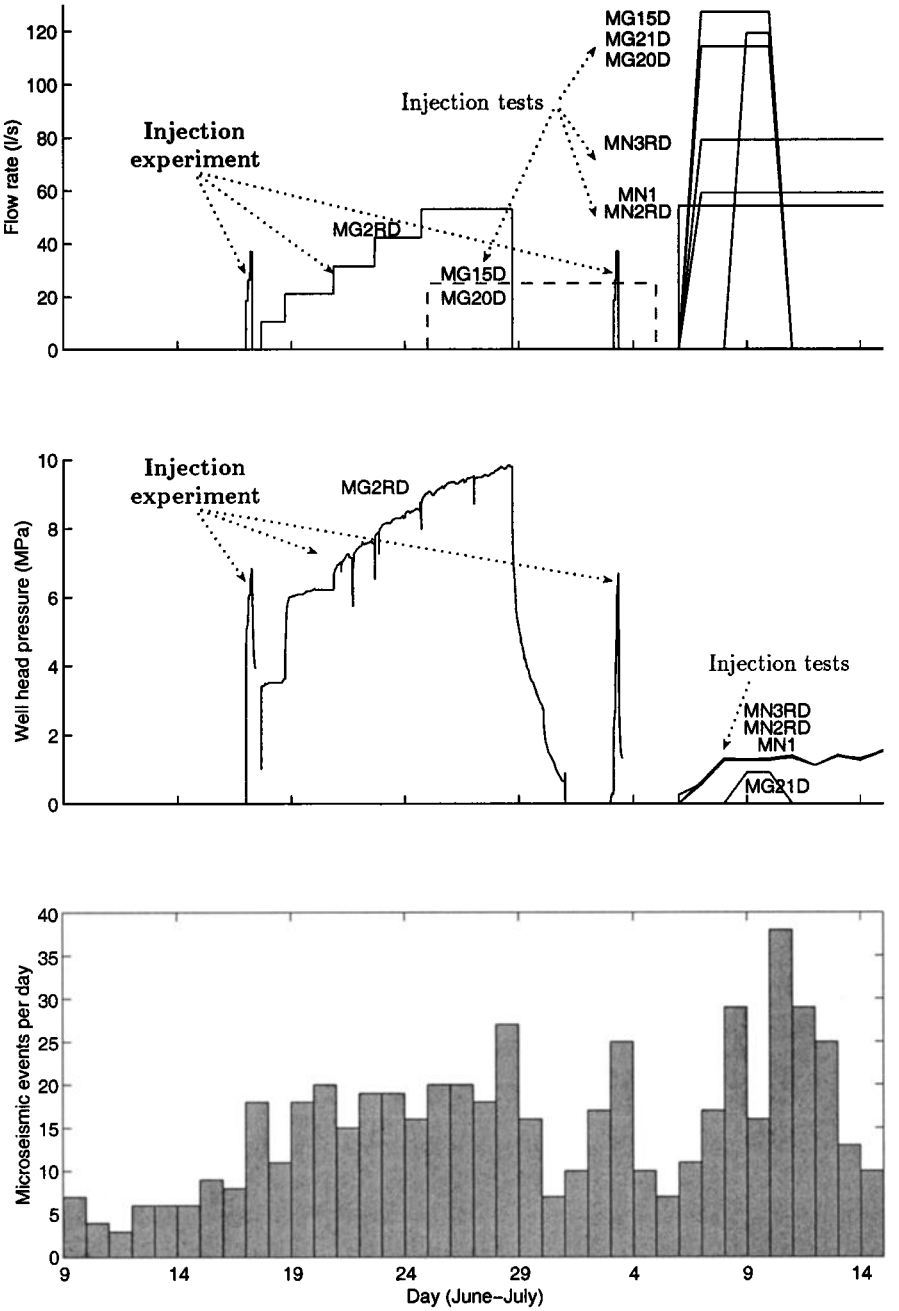


Figure 2. Injection flow rate, wellhead pressure, and level of microseismicity monitored during June-July 1997 for the injection experiment in well MG2RD and for the injection tests in wells MG15D, MG20D, MG21D, MN1, MN2RD, and MN3RD. The increase in flow rate, for MG2RD, is followed by the increase in wellhead pressure and seismicity level and suggests that induced seismicity results from a pore pressure increase. The two short peaks, observed before and after the MG2RD injection, correspond to pumping tests for the experiment.

stone formation is a thick sequence of predominantly fine clastics such as claystone, siltstone, and sandstone and is assumed to exhibit plastic behavior. The Mahiao Sedimentary Complex is a sedimentary conglomerate containing quartz and monzodiorite fragments with unmetamorphosed sandstones and siltstones and was anticipated to exhibit a more brittle behavior than the Mahanagdong Claystone formation.

A survey conducted in the well before the injection experiment has shown that the well has a diameter reduction from 12.7 to 8.9 cm at around 1880 m bgs, i.e., slightly above the depth where the borehole intersects the Central Fault Line. It was hoped that below this depth, the liner was still open at its nominal diameter.

The goal of the injection experiment was to stimulate, by shearing and cooling, the preexisting fractures that

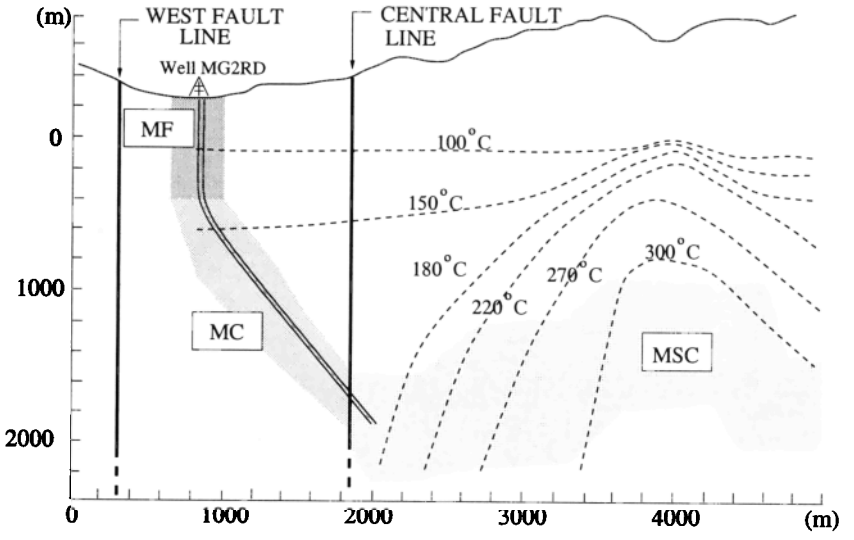


Figure 3. Cross section of well MG2RD (direction NNE) that crosses the Central Fault Line 1980 m below ground surface. The well intersects an andesitic formation (MF), a thick sequence of predominantly fine clastics (MC), and a sedimentary conglomerate (MSC) after it has crossed the fault (modified from *Delfin et al.* [1995]). Stratigraphy and isotherms were deduced from borehole loggings. Vertical depths (meters) are reported with respect to sea level.

intersect the well in the MSC formation. The injected fluid was river water at a temperature of 25°C. Starting on June 19 with a flow rate of 10.6 L/s for 24 hours, the flow rate was increased by 10.6 L/s increments every other day (Figure 2) so as to reach 53 L/s after 8 days of pumping. Because of the pumping capacity and the wellhead characteristics the flow rate had to be kept constant at 53 L/s during the last 4 days of the test. The stimulation ended on June 30 with a total injected volume estimated at 36,000 m^3.

After 11 days of pumping, the well was closed for 24 hours. Then, it was opened and logged with a Kuster tool (pressure and temperature gauges) during the flow back (from 1850 m bgs just above the liner reduction). The temperature log (Figure 4) shows that the temperature was drastically reduced by the injection over the entire length available for logging ($\sim$ 75°C). The lowest temperature (71°C) is found at the maximum accessible depth and demonstrates that most of the flow reached below this depth into the Mahiao Sedimentary Complex. The thermal anomaly, which occurred during injection and is identified between 1400 and 1500 m bgs, is a small inflow associated with minor losses within the Mahanagdong Claystone.

For exploitation purposes and independent of our experimentation, injection tests were conducted in six wells in the vicinity of MG2RD. In particular, two wells, MG15D and MG20D (Figure 1), have been sporadically used, starting on June 25, without any flow rate and wellhead pressure monitoring. Then a regular injection program started, on July 5, in the six wells, MG15D, MG20D, MN1, MN2RD, MN3RD, and MG21D. Initially, large injection flow rates (up to 127 L/s) have been imposed. Yet they have been associated with only small wellhead pressures (up to 1.5 MPa), a feature which demonstrates the initial high permeability of these wells. The flow rates and wellhead pressure are summarized on Figure 2. For later use in the paper, we need an evaluation of a lower bound of the total injected volume. In this respect, it is safe to assume that during the June 25 to July 5 period, the injection flow rate for wells MG15D and MG20D was larger than 1/4 of that used during the July 5-15 period. Consequently, the total injected volume in these wells, during the entire experimental period (June 25 to July 15), has been estimated at 327,000 $\pm$ 20,000 m^3. It is worth mentioning that a large decline of the injection flow rate capacity was observed in MN3RD (79 to 20 L/s), 2 months after the experimental period, as well as a slight decrease in MN2RD (54 to 42 L/s) and MG21D (119 to 108 L/s).

3. Monitoring Seismicity

3.1. Recording Networks

The microseismic activity in Tongonan has been monitored with various types of surface stations. First, a permanent telemetered network of seven stations was installed by the Philippine Institute of Volcanology and Seismology (PHIVOLCS) between February 1996 and July 1997 in order to continuously monitor the local seismicity. In addition, a seven-station telemetered network and four independent stations were deployed by Ecole et Observatoire de Physique du Globe de Strasbourg (EOPGS) for a survey conducted during October-November 1996 and for the injection experiment during the June-July 1997 period. Location of the various stations is shown on Figure 1c. The stations of both telemetered networks were equipped with a single ver-

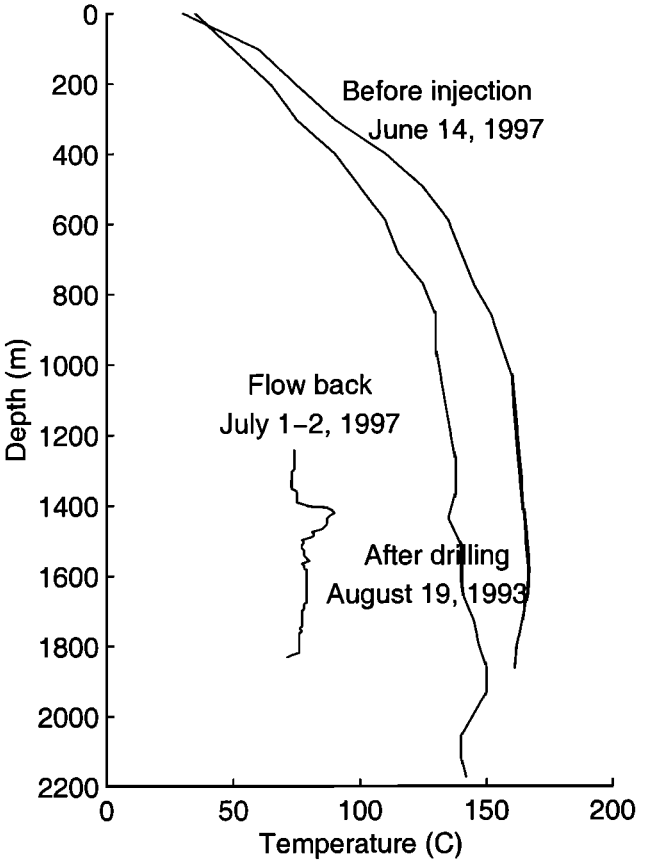


Figure 4. Thermal logs conducted, in MG2RD, after drilling, before the beginning of the injection experiment, and after the injection (flow back of water). A thermal anomaly is clearly identified around 1980 m bgs where the well intersects the fault (August 19, 1993, log). Temperature has been drastically reduced by the injection experiment over the entire length of the well (July 1-2, 1997, log).

tical 1-Hz seismometer. Signals were transmitted by UHF to a central recording system and recorded simultaneously with a GPS-synchronized time signal. Signals recorded with the PHIVOLCS network were digitized at a rate of 75 samples per second (sps) and signals recorded with the EOPGS network at a rate of 185 sps. The other four independent stations (three components, 1 Hz, 185 sps) had their own trigerring and time recording system. For these stations, a GPS-synchronized time was added every 4 days. Using this as calibrations, we estimate the timing accuracy to 0.02 s.

The geometry of the network was chosen so as to study seismicity along the actively creeping fault segment of the Philippine Fault as well as the seismic activity induced by the injection experiment. The whole set of stations was installed in a dense network along the West and Central Fault Lines, oriented roughly NNW-SSE (Figure 1c). The azimuthal coverage of the network was limited by the inaccessible mountain to the east. The area covered by all the stations was about 20 km by 10 km in the NNW and ENE directions, respectively. It should be noted that the network elevation reference has been taken as the elevation of the lowest station, some 400 m above sea level. The elevation of the highest station was 1015 m above sea level.

Depending on the deployed instruments, four periods are identified: period 1 (February-August 1996) and period 3 (December 1996 to May 1997) during which only the PHIVOLCS network was operated, and period 2 (50 days, October-November 1996) and period 4 (43 days, June-July 1997) during which the complete set of 18 stations was installed. In this present study, seismicity analysis is focused on periods 2 and 4, i.e., before and during the experimental injection period.

3.2. Microseismic Activity

A total of 1760 events were detected in the vicinity of the network during periods 1, 2, 3, and 4, with ~500 events for period 1, 240 for period 2, 460 for period 3, and 560 for period 4 with coda magnitude range between 0.5 and 3. Events of periods 2 and 4 were first located with the HYPOINVERSE program [*Klein*, 1989] using an updated a priori 1-D four-layered velocity model (model 1, Table 1). The updated a priori 1-D model had been previously established, following *Kissling et al.* [1994], with period 1 data and an a priori 1-D model based on geologic informations. Travel times were corrected for station elevation by assuming the same near-surface crustal velocity as layer 1. No correlation between travel time residuals and station elevations has been found. Events locations were considered well constrained when their RMS arrival time residuals were <0.15 s; for all selected events the mean RMS value is 0.05 s. Events are distributed down to 10 km. The locations of well-constrained events for period 2 and 4 are presented on Figure 5. They correspond to the first step for the selection of a consistent data set for further analysis of the seismicity.

4. Tomography Inversion

4.1. Initial Settings and Inversion Procedure

Travel times used in the tomographic inversion were selected from events which met the following criteria:

Table 1. One-Dimensional a priori Velocity Models

	1-D Model 1[a]		1-D Model 2[b]	
Z, km	V_p, km/s	V_p/V_s	V_p, km/s	V_p/V_s
0	3.56	1.73	3.30	1.54
1.5	3.75	1.73	3.74	1.71
3	4.33	1.73	4.35	1.64
5	5.20	1.73	5.07	1.69
10	6.20	1.73	6.21	1.73
40	8.00	1.73	8.00	1.73

[a]Model 1 was used for previous locations.
[b]Model 2 was computed for the use of a priori information for the tomography inversion.

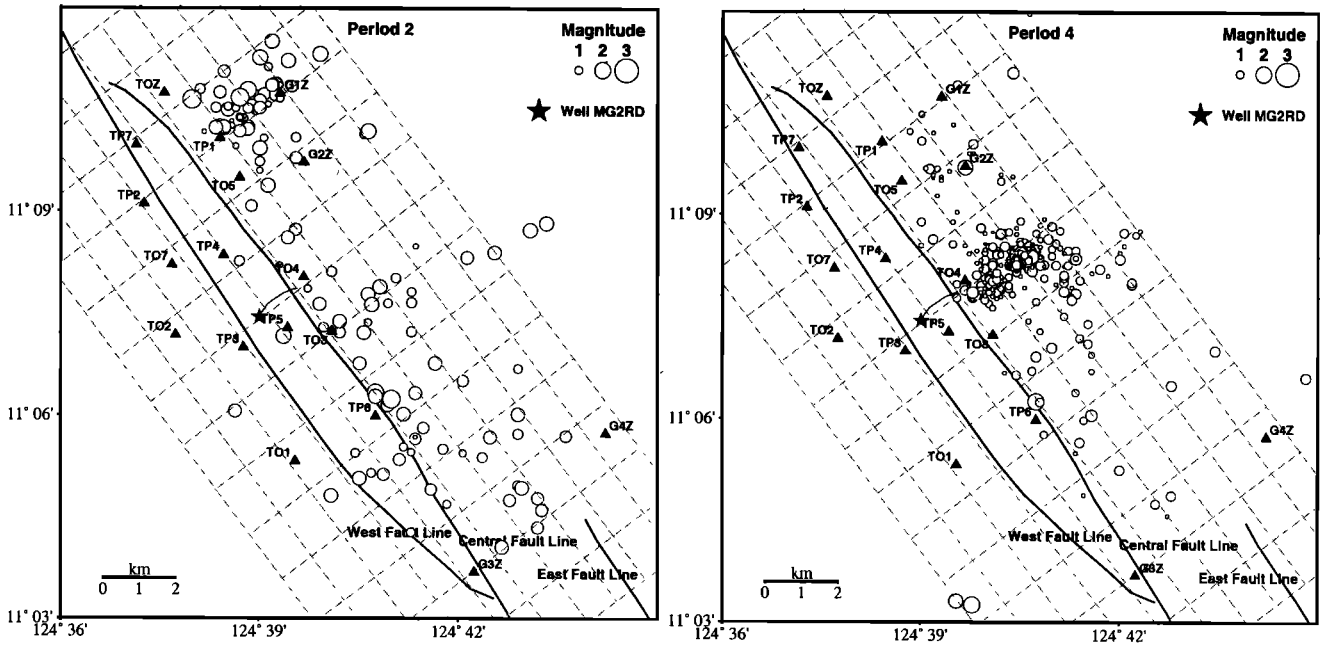


Figure 5. Map of the epicenters (circles), seismic stations (triangles), well MG2RD (solid dot and line), and model grid spacing used in tomographic study. The 141 events and 292 events were selected for periods 2 (October-November 1996) and 4 (June-July 1997), respectively. The 3-D velocity values are calculated at the intersection points (nodes) of the spaced, 1 × 1.5 km, horizontal grid. The vertical grid spacing is 1.5 km.

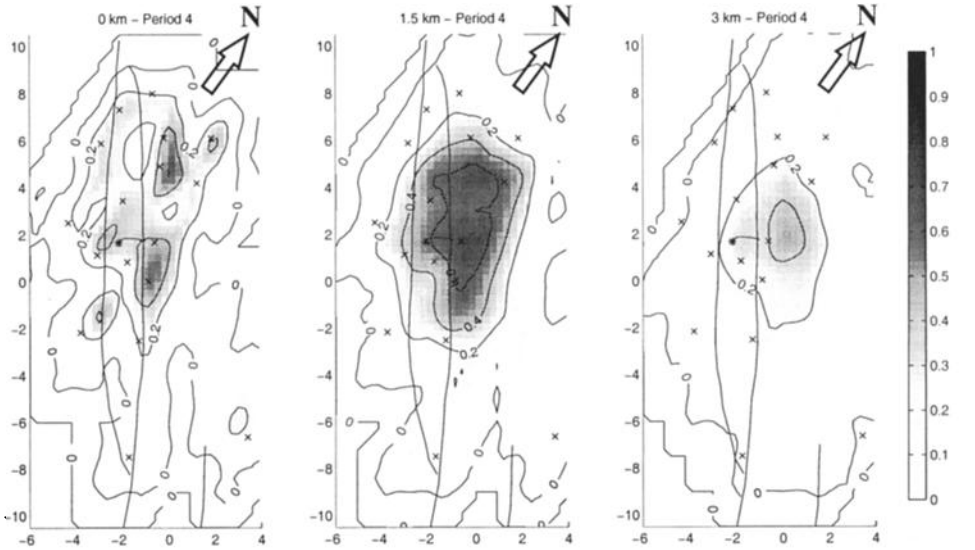
number of P readings ≥ 7, number of S readings ≥ 2, RMS ≤ 0.15 s, horizontal standard error ≤ 0.5 km, vertical standard error ≤ 0.8 km. This gave 292 events for period 4 and a data set of 5291 travel times (3939 P, 1352 S). Although the number of S travel times is insufficient for giving a well-resolved S velocity model, they constrain hypocentral depths and hence the inversion. Events from period 2 were selected with the same criteria. This gave 141 events (3137 travel times, 1743 P, 1394 S). Despite the fewer number of events for period 2, the spatial coverage is of better quality for this period since events are not concentrated close to injection site (see Figure 5).

The selected travel times for P and S waves were inverted in order to determine simultaneously earthquake locations and the 3-D velocity structure beneath the seismic array. The tomographic inversion method (SIMULPS10) is an iterative damped least squares technique which was originally developed by *Thurber* [1983] and modified by *Eberhart-Phillips* [1990]. The method has been applied to active faults area by *Eberhart-Phillips* [1986, 1990, 1993] and *Dorbath et al.* [1996]. A modified version of the computer program (SIMULPS12) that can invert both P and S-P times [*Thurber*, 1993; *Evans et al.*, 1994] was also applied to geothermal areas by *Foulger and Miller* [1995] and *Julian et al.* [1996].

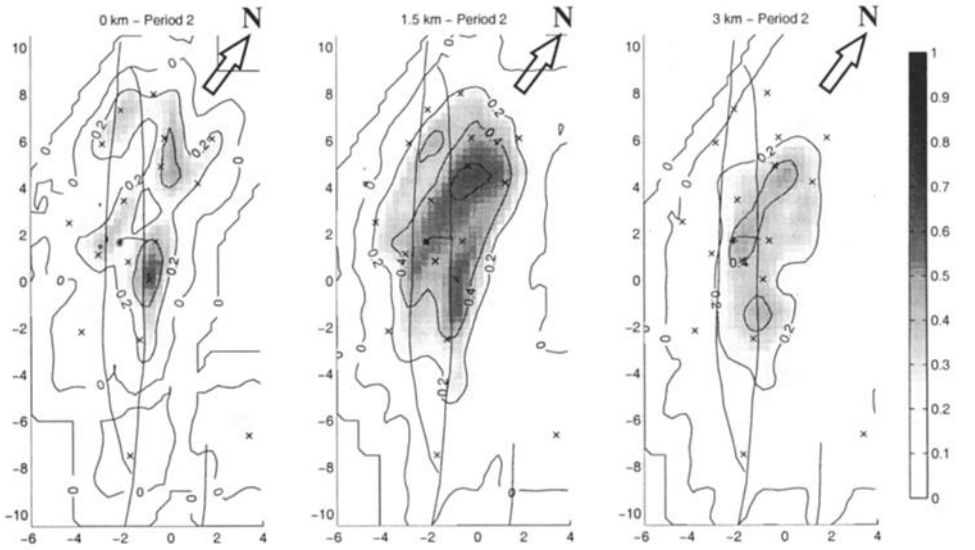
As detailed by *Eberhart-Phillips* [1986], the velocity of the medium under investigation is parameterized by assigning velocity values at the intersections (grid points) of a nonuniform, three-dimensional grid. The propagation velocity for a point along a seismic ray path and the velocity partial derivatives are computed by linearly interpolating between the surrounding eight grid points. The area covered by the stations, the hypocenters, and the three branches of the Philippine Fault extends some 20 km along the faults and 10 km across them. The coordinates are chosen so that the Y axis is oriented parallel to the average strike of the Philippine Fault in this region (37° west of north). The grid frame is represented on Figure 5.

Next, a precise initial 1-D velocity model has been determined. We inverted the travel times from periods 2 and 4, with the preliminary 1-D model used for the first location determination as an initial model (model 1, Table 1), so as to determine a minimum 1-D velocity model [*Kissling et al.*, 1994]. This inversion led to a variance reduction of 27% and 21% for P and S waves residuals, respectively. The resulting one-dimensional model is shown in Table 1 (model 2).

Once the general frame for the inversion was set up, different inversions were carried out with different grid spacings, different damping parameters, and different initial velocity models. The grid spacings were chosen so as to resolve small velocity perturbations associated with the injection experiment as well as velocity contrasts across the two fault segments (WFL, CFL), which are only 2 km apart from each other. We used a regular 1 × 1.5 km grid spacing along the horizontal X and Y axis, respectively, in order to have reasonable resolution at most grid points. The vertical nodes extend from 0 to 10 km (maximum depth of seismicity) with intermediate nodes at 1.5, 3 and 5 km.



(a) Period 2



(b) Period 4

Figure 6. Diagonal elements of the resolution matrix for the final models of (a) period 2 and (b) period 4, at layer node 0, 1.5, 3 km (plan view). Resolution reflects station spacing and distribution of seismicity. The inversion grid has been rotated from 37° NE. Contours units are 0.2. Stations are displayed with crosses, and MG2RD wellhead is marked with a star mark.

The elevation reference is that of the lowest station, i.e., 400 m above sea level. When grid point spacings were varied (1 × 1 km, 1.5 × 1 km) or grid point locations were translated by 0.5 km (X or Y), the general shape and location of velocity anomalies were not modified. In this tomographic inversion, one has to find the damping parameter that gives the best compromise between data variance reduction and the model variance. We performed inversions using 10 different values for the damping parameter (between 2 and 100 s^2 km^{-1}) and analyzed "trade-off curves" between resolution and standard errors [*Evans and Achauer*, 1993]. From these tests the damping parameter was chosen so that the diagonal terms of the a posteriori covariance matrix would be smaller than 2% of the mean P velocity of each considered layer for period 4. Then we tested the sensitivity to the initial velocity model for the three-dimensional inversion. Tests were done with various initial velocities. An alternative a priori model (model 3) with depth spacing every kilometer was determined as for model 2. After different three-dimensional inversions with starting models 2 and 3, the mean P velocity and the pattern of velocity variations in each layer were nearly identical for the two models down to a depth of

5 km. They differed by at most 6%, and this occurred at the surface where velocity constraint is minimal because of insufficient coverage. Moreover, the differences in the epicenter locations were generally <300 m. In summary, we find that the inversion process, for these data, is robust, in that the differences in the results are not very sensitive to the initial velocity model and the grid spacing.

4.2. Inversion Results

After five iterations, the P data variance was reduced by 51% from 0.010 to 0.005 s^2 for period 4 and by 42% from 0.018 to 0.010 s^2 for period 2. The diagonal elements of the resolution matrix for the three upper layers for periods 2 and 4 are shown on Figure 6. Values for the diagonal terms of the resolution matrix range from 0 (no resolution) to 1 (perfect resolution). The resolution at the surface reflects the station distribution: it is high close to the stations and low elsewhere. The resolution improves with depth for the 1.5 and 3 km depth node layers, where a complete zone can be defined as being well resolved. The highest resolution is observed for period 4 at depth 1.5 km with values close to 0.7 (Figure 6b). Deeper resolution decreases rapidly, but a zone with resolution >0.2 can still be identified. The resolutions for the two periods are quite similar in the central region and indicate no significant differences in sampling.

Standard errors for velocity depend on resolution and on mean velocity. Standard errors remain <2% of the mean P velocity for period 4 data (73% of data <1% at 3 km depth) and 4% for period 2 data (72% of the data <3%). For the model space where resolution is >0.5, velocity errors are close to 0.06 km s^{-1} at the surface, 0.07 km s^{-1} at 1.5 km and 0.09 km s^{-1} at 3 km depth (period 4). The mean horizontal error for event relocation is ~60 m, and the vertical error is ~100 m.

4.2.1. Earthquake locations. Epicenters of the relocated events for period 4 (43 days of recording) are displayed on Figure 7. A comparison between the initial and the final epicenter locations shows modest differences: 59% of the 292 relocated events differ by <0.5 km from the initial epicenter, 87% differ by <1 km. The differences in depth are quite similar, 64% of the events differ by <0.5 km from the initial depth, and 83% differ by <1 km. Despite these small shifts, the main seismicity cluster exhibits a notable difference in shape and shows more individual clusters (Figures 5 and 7).

Most microseismic events are located to the east of the Central Fault Line, within the geothermal reservoir, with only very few events along the Central Fault Line and to the west of it. The recording period (Figure 7) has been divided into three subperiods in order to separate the seismic activity induced by the MG2RD injection experiment from that induced by other field activities before or after. In the vicinity of MG2RD, no significant activity was observed before June 18; microseismic activity is observed only after the injection has started. Once the stimulation ends, the associated seismic cloud disappears. The absence of seismicity and field activity prior to and after the experiment shows that the observed seismicity in the direct vicinity of the well, during the days of pumping, is linked only to the MG2RD stimulation.

More precisely, the level of microseismicity per day for period 4 has been displayed along with flow rate and wellhead pressure for the various injection activities (Figure 2). For the MG2RD experiment a clear temporal correlation can be observed with the increase in the number of microseismic events and the increase in wellhead pressure. Moreover, just after the end of the stimulation, the level of microseismicity decreases immediately and follows the monitored decrease of pressure. The increase in wellhead pressure and the fact that most of the flow reached into the Mahiao Sedimentary Complex suggest strongly that pore pressure has been increasing in the MSC formation. This mechanism has been often described in the literature [e.g., *Pearson,* 1981; *Pine and Batchelor,* 1984; *Fehler,* 1989; *Cornet,* 1992]. Other mechanisms for geothermal sites such as fluid extraction [*Segall,* 1989] or thermoelastic effects [*Mossop,* 1998] have also been associated with induced seismicity but are not considered relevant here.

Figure 7 also indicates that the stimulation has not induced any event along the Central Fault Line. The geometry of well MG2RD is known with an accuracy of 60 m, and the wellhead location is known to within 50 m. Hence the uncertainty of the distance between the location of the well and the location of an event is close to 170 m. The earthquake activity remains confined within a volume which extends from the bottom of the well down to ~4 km (3.6 km below sea level). No event has been induced in the upper section of the well above the Central Fault Line. No clear downward migration with time can been identified from the analysis of the seismic cloud. The absence of seismic event along the fault during the injection experiment may reflect either an absence of change in pore pressure or the occurrence of aseismic slip.

In addition, wells MG15D and MG20D exhibit few induced seismic events from June 25 to July 4. These are clearly confined to the extremity of each of these wells and are fairly distinct from the MG2RD seismic cloud (Figure 7). The regular injection activities in MG15D, MG20D, MN1, MN2RD, MN3RD, and MG21D, after July 4, have induced seismic activity local to these wells (Figure 7). Although the total injected volume is more important in the regular injection program than that of the MG2RD stimulation, wellhead pressure at the other wells is much lower (close to 1 MPa) than that at MG2RD (~9 MPa at the end of the experiment), a feature which may explain why the correlation between the level of microseismicity and the increase of pore pressure is not as clear for these wells and why the level of

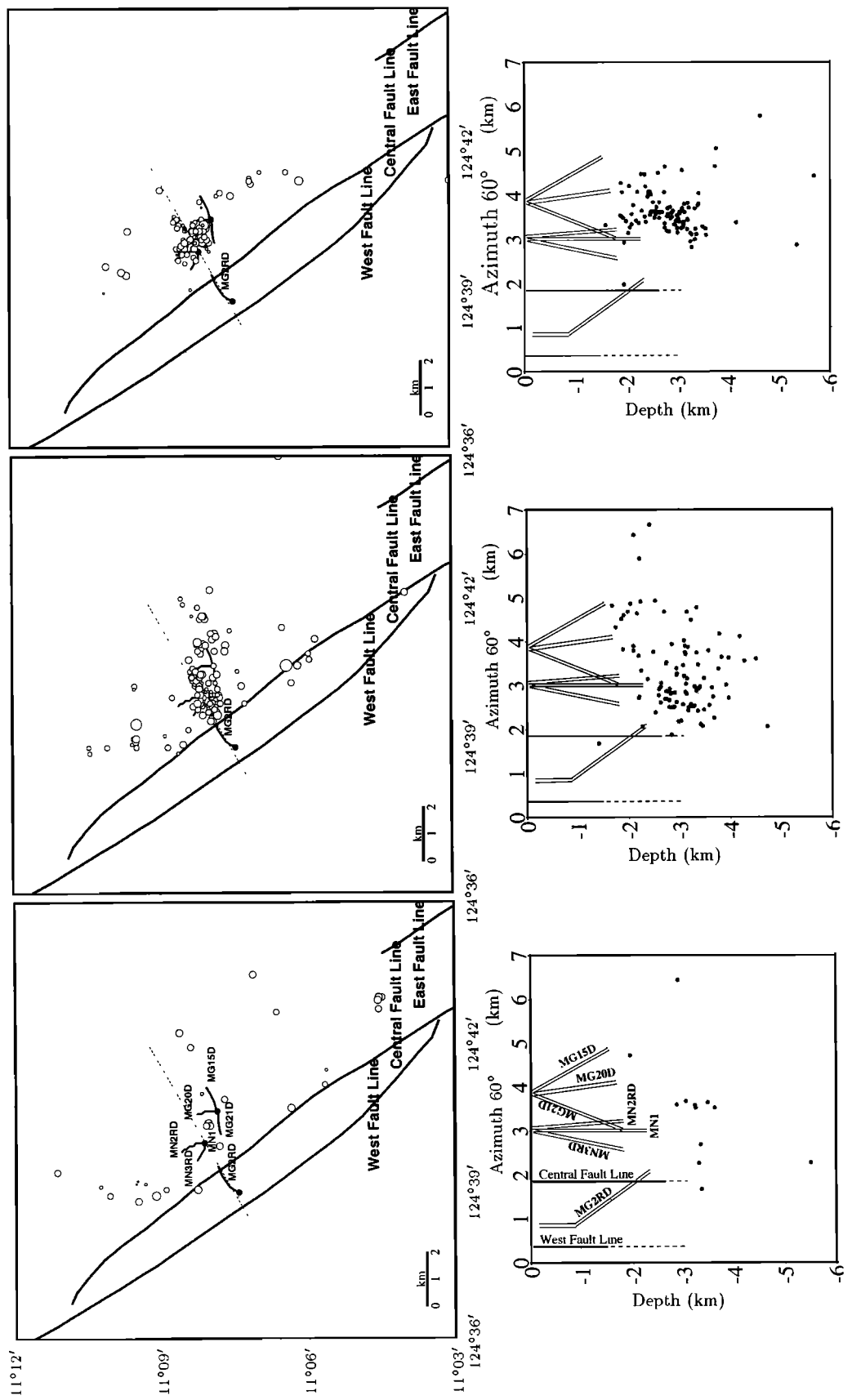


Figure 7. The relocated microseismic events observed from period 4 have been split into three subperiods, before, during, and after MG2RD injection experiment. More than 300 induced events have been recorded in the vicinity of well MG2RD during the experiment. No event has been induced along the Central Fault Line. The injection tests in wells MG15D, MG20D, MG21D, MN1, MN2RD, and MN3RD have also induced microseismic events in the vicinity of the wells, mostly between July 5 and 15. Cross sections (azimuth 60°) exhibit the same features. On site, most microseismic events are located to the east of the Central Fault Line, within the geothermal reservoir, with very few microevents along the faults.

seismicity related to MG2RD is so high. The seismicity associated with the other wells extends also from the bottom of the wells down to ~3.5 km.

The map of relocated events for period 2 (Figure 8) exhibits the same features as for period 4: Most microseismic events are located to the east of the Central Fault Line, within the geothermal reservoir, with only very few events along the fault and to the west of it. In addition, events recorded for periods 1 and 3 (14 months) have also been relocated using the a priori 3-D velocity model for period 2 (Figure 8). These observations have to be interpreted with care because of the lower source location accuracy due to the fewer number of stations. In the northern part of Tongonan, where the azimutal coverage of the stations is the best, seismicity is located within the geothermal site with most of it at shallow depth (1-5 km), and very few events are located along the West and Central Fault Lines. Southwest to the network, events occur at greater depth (mostly 4-7 km) but are more scattered and cannot be easily associated to any particular structure.

4.2.2. Velocity model. The P wave velocity models in the first three node layers is presented on Plates 1a and 1b for periods 2 and 4, respectively. They have been contoured after interpolation. On these Plates 1a and 1b, the zones with a resolution <0.2 for both periods were not represented. This mask allows us to keep only the most reliable information for both models. At greater depths the well-resolved zone tends to shrink.

The overall pattern of anomalies found in the two models, on Plates 1a and 1b, is similar, and particular features may be observed. At the surface (0 km) the well-resolved information is concentrated in the vicinity of the stations. The low V_p velocity zones (-10 % from the mean V_p at the layer) are observed at layer 1.5 km directly beneath the Mahiao, Malitbog, and Mahanagdong areas, which correspond to the most productive zones found in the geothermal field. For example, significant low velocities are observed in Mahiao area where hot fluid upwelling occurs. The low velocity beneath Mahanagdong is also observed for the 3-km layer. A

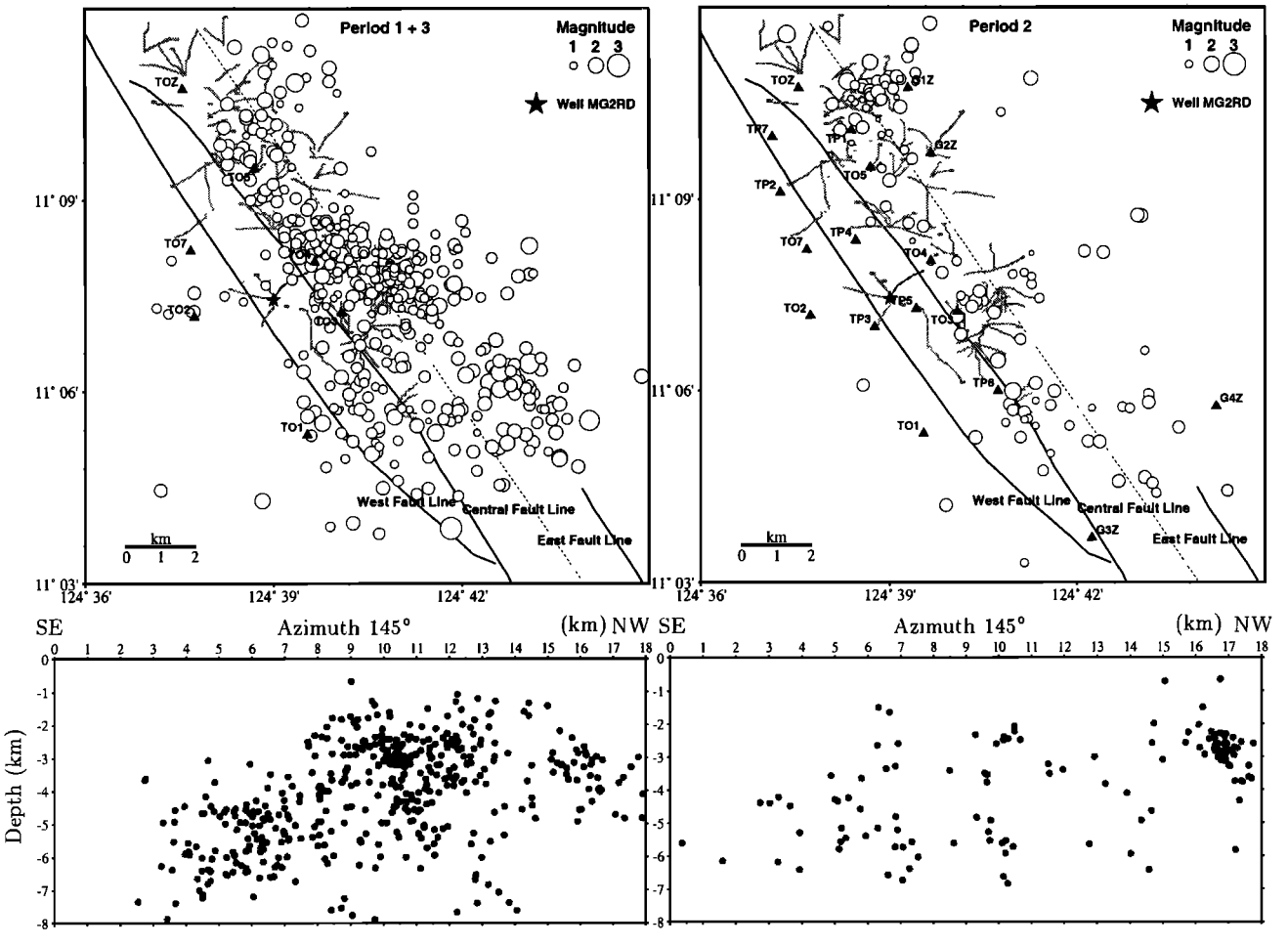


Figure 8. (left) Seismic events for periods 1 and 3 (7 stations, 14 months) have been relocated using the 3-D velocity model determined for period 2 (469 events). (right) Relocated seismic events for period 2 are also displayed, as well as azimuth 145° cross sections. The horizontal projections of the geothermal wells are also shown shaded.

high V_p zone is located in the Bao valley, where no flow of high-temperature fluid exists within the impermeable basement rocks and the Mahanagdong Claystone [*Delfin et al.*, 1995]. A small low-velocity zone can be observed on cross sections of both models beneath the Central Fault Line (see Y=1.5, Plate 2).

The most prominent difference is observed on node $X = 0$, $Y = 1.5$ at layer 3 km for period 4. It is a high P wave velocity zone in the vicinity of the injection wells (Plate 1b). This anomaly, located close to Mamban area, is also slightly seen in the 1.5 km layer. This high-velocity zone is not observed for period 2 (Plate 1a). The feature appears more clearly on a cross section (see Plate 2, $X = 0$, $Y = 1.5$). For this node, at the 3 km layer depth, the perturbation of the P wave velocity shows a 14% increase between the two periods (from 4.44 to 5.04 km s^{-1}, hereinafter called period 4 anomaly). On Plate 1a, one can also observe a high-velocity zone (hereinafter called period 2 anomaly) centered 2 km north of the first anomaly. This period 2 anomaly is located close to a lower-resolution zone and is not present in period 4.

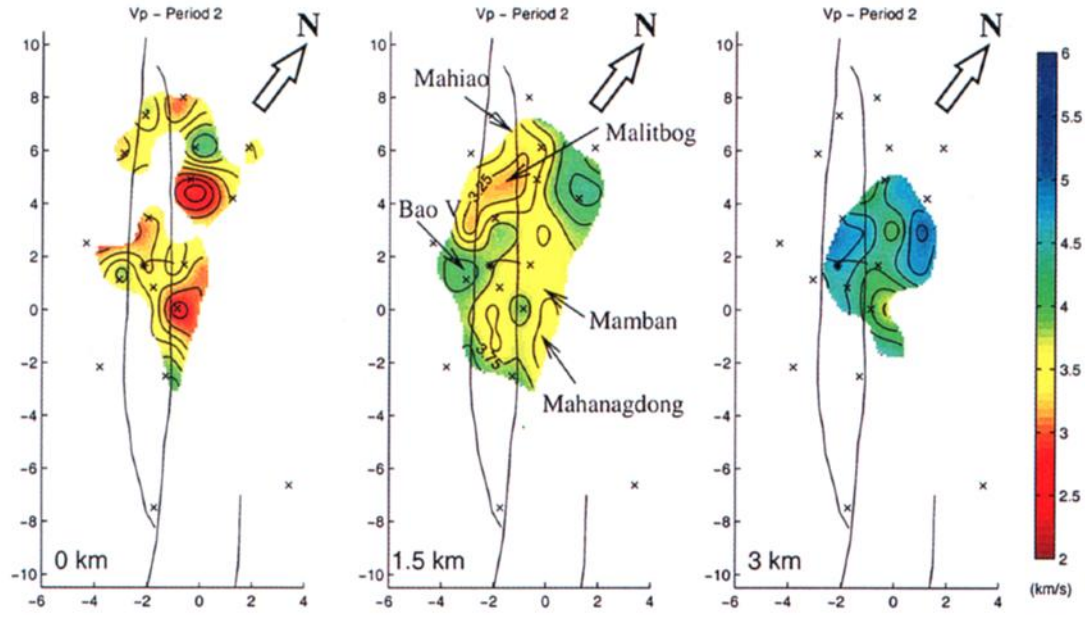
A question may be raised concerning the reality of these velocity anomalies. The two fields experiments of periods 2 and 4 have provided two independent data sets with the same network geometries and instrumentation. Further, for both data sets the inversion methods and parameterization are the same. In the models the difference between the mean V_p value in each layer is <0.03 km s^{-1}. The similarity in the overall velocity pattern for both inversions gives us some confidence in the results. Computations of V_s and V_p/V_s ratio velocity with computer codes SIMULPS10 and SIMULPS12, repectively, do not yield well-resolved models, but the overall pattern of the two models are very similar. Results from SIMULPS12 show a high V_p/V_s ratio at the location of the period 4 anomaly.

Before discussing physical processes that would lead to such velocity changes, we describe numerical tests which have been conducted in order to assess the robustness of these observations. First, different subsets of the two data sets have been used in order to insure that the models are not biased by the poor quality of some data. For each data subset the general pattern was found to be identical to the model derived from the complete data set. Accordingly, the existence of an artifact induced by erroneous data is excluded. Second, an important concern is to insure that different ray path distributions from periods 2 and 4 would sample the region of interest sufficiently well for resolving both anomalies.

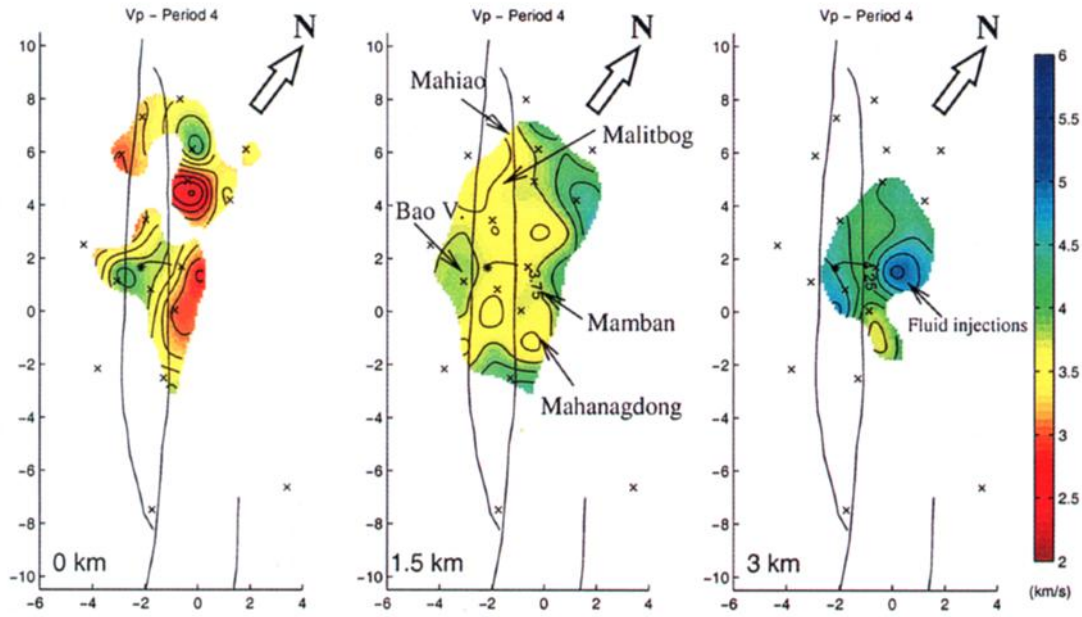
The first test consist of inverting the data from period 2 with an a priori 1-D model that includes the observed perturbation of period 4 ($X = 0$, $Y = 1.5$, Plate 3a). If the anomaly is erased after computation, that would mean that enough ray paths have resolved the zone and corrected it from the introduced a priori anomaly. In practice, 12 nodes (layers 1.5 and 3 km) of the observed anomaly were included in the previous a priori 1-D model (model 2). Plate 3a shows the new a priori model and Plate 3b shows the result of the new inversion for period 2 for the 3-km layer. Clearly, it is observed that the a priori anomaly, at the location of the induced seismicity, has been "erased". Moreover, the velocity pattern is the same as that shown on Plate 1. Layer 1.5 km exhibits similar results. Hence it is concluded that the ray paths coverage is sufficient to resolve zones of interest with period 2 data and that the period 4 anomaly was not present at that time; that is, the model space at the location of the period 4 anomaly is well constrained. More quantitatively, a second test has been designed to observe the influence of the ray paths distribution on the location and amplitude of two anomalies in the inversion process. We prepared an a priori model as follows: a 15% P wave velocity perturbation has been introduced at the location of the two nodes corresponding to the period 2 and period 4 anomalies in an a priori homogeneous model (4 km s^{-1}, see Plate 4a). Then, the two hypocenter distributions from periods 2 and 4 have been used separately to calculate synthetic travel times for the new a priori model. Next, the synthetic travel times of both periods have been inverted with an a priori homogeneous model (4 km s^{-1}) in order to try to reconstruct the introduced anomalies. Results of this process, for the 3-km layer, clearly show (see Plates 4b and 4c) that the period 4 anomaly is well reproduced in location for the two periods and both inversions indicate similar amplitude attenuation. The designed 15% anomaly is recovered, for both models, as a 4% velocity anomaly. This confirms the result of the previous test. Had the period 4 anomaly been present during period 2, the tomography method would have outlined it in the same manner as in period 4. Hence comparison of the models within the induced seismicity zone can be conducted with greater confidence. It is concluded that the injection of water in well MG2RD, and in other nearby wells, has induced an increase of P wave velocity in the vicinity of the wells, but evaluation of amplitudes has to be considered with care.

However, it should be noted that Plates 4b and 4c show that the amplitude of the period 2 anomaly was not reconstructed in the same manner for the period 2 and period 4 data distributions, so that it is difficult to compare them. In addition, the reconstruction of the period 2 anomaly has introduced some smearing for the period 2 data set. Hence the existence of period 2 anomaly is questionable.

The second test has also been repeated with a data set of 231 earthquakes generated on a uniform grid at 6 km depth. In this test the amplitude of the designed anomaly is recovered as well as a 10% velocity anomaly. This suggests that our model computation might have underestimated the real amplitude of the anomaly because of the seismicity distribution.



(a) Period 2



(b) Period 4

Plate 1. Three-dimensional P wave velocity model (km s^{-1}) (a) for period 2 and (b) for injection period 4, at layer node 0, 1.5, 3 km (plan view). The inversion grid has been rotated from 37° NE. Color scale represents P velocities in between 2 and 6 km s^{-1}. Only results that exhibit a resolution higher than 0.2 for both periods 2 and 4 are shown, in order to select reliable information for both models (see text). P wave velocity anomalies can be identified between the two models, especially near the injection sites.

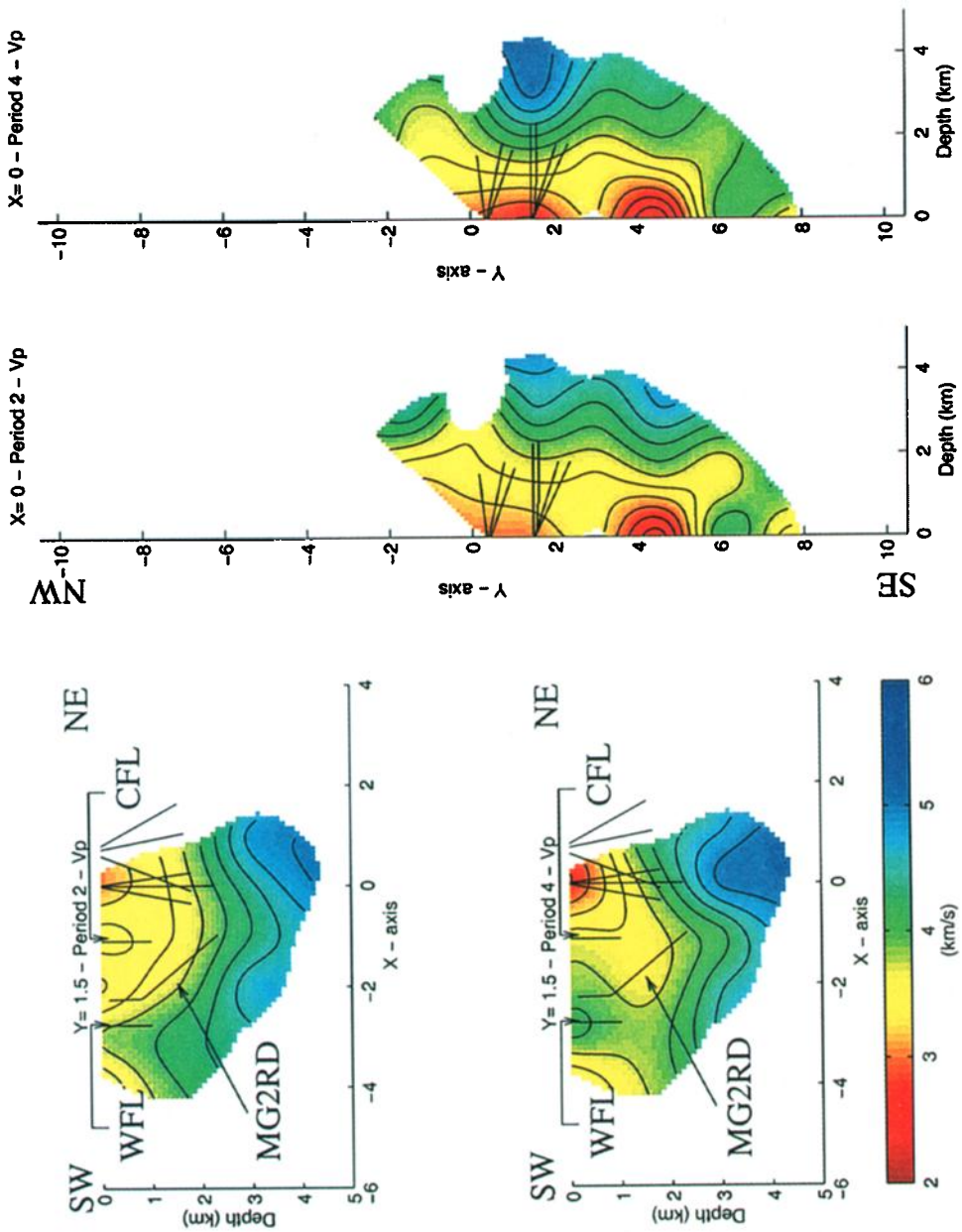


Figure 10:

Plate 2. Cross sections of the 3-D velocity model (km s^{-1}) across ($Y = 1.5$) and along ($X = 0$) the fault. The period 4 anomaly is clearly identified (*see text*). Depths are given with respect to the network elevation reference, i.e., 400 m above sea level.

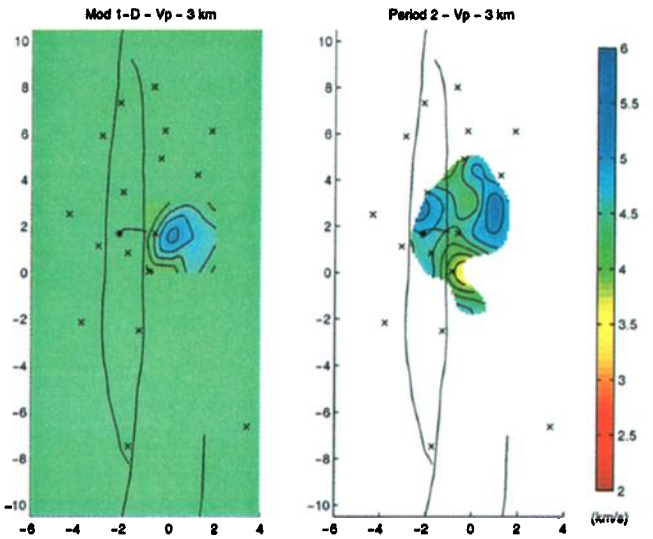


Plate 3. Test for the detected period 4 anomaly. (left) Data from period 2 were inverted again using an a priori model where the anomaly of period 4 has been introduced in an homogeneous layered model (1D) at layer node 3 km. (right) Results show the resulting V_p model (layer 3 km). The introduced anomaly has been removed out from the a priori model.

At other geothermal sites, low V_p/V_s velocities have also been reported [*Julian et al.*, 1996] but no evident anomaly was observed on V_p alone. In our case the results from the velocity models have shown that changes in fluid content because of injections (period 4 anomaly), have induced at least a 14% increase of the P wave velocity in a rock volume distributed in depth ranging between 1360 and 2860 m bgs.

5. Discussion

5.1. Seismicity and Philippine Fault

The microseismicity observations during one and half year have shown that very few events (magnitude 0.5-3) occurred, in Tongonan, along the Central Fault Line and the West Fault Line. Moreover, the stimulation experiment by forced fluid injection across the Central Fault Line did not induce any microevents along the fault. GPS measurements that have been conducted before and after the experiment (June and July 1997) do not yield any detectable displacement along the fault that may indicate any faster aseismic slip because of the experiment. In between 1991 and 1997, less than 10 earthquakes of magnitude 4 and none with larger magnitude have been recorded along the 50-km segment of the Philippine Fault in northern Leyte (11°05′-11°30′N) by the Philippino national network or worldwide seismicity.

Only one earthquake of magnitude 5.4 was located 12 km east to the East Fault Line on May 17, 1993 (Harvard epicenter: 11.05°N, 124.84°E). This event was attributed to the Philippine Fault after a seismic survey recorded 70 aftershocks in the vicinity of the East and Central Fault Lines, south to Tongonan (latitude

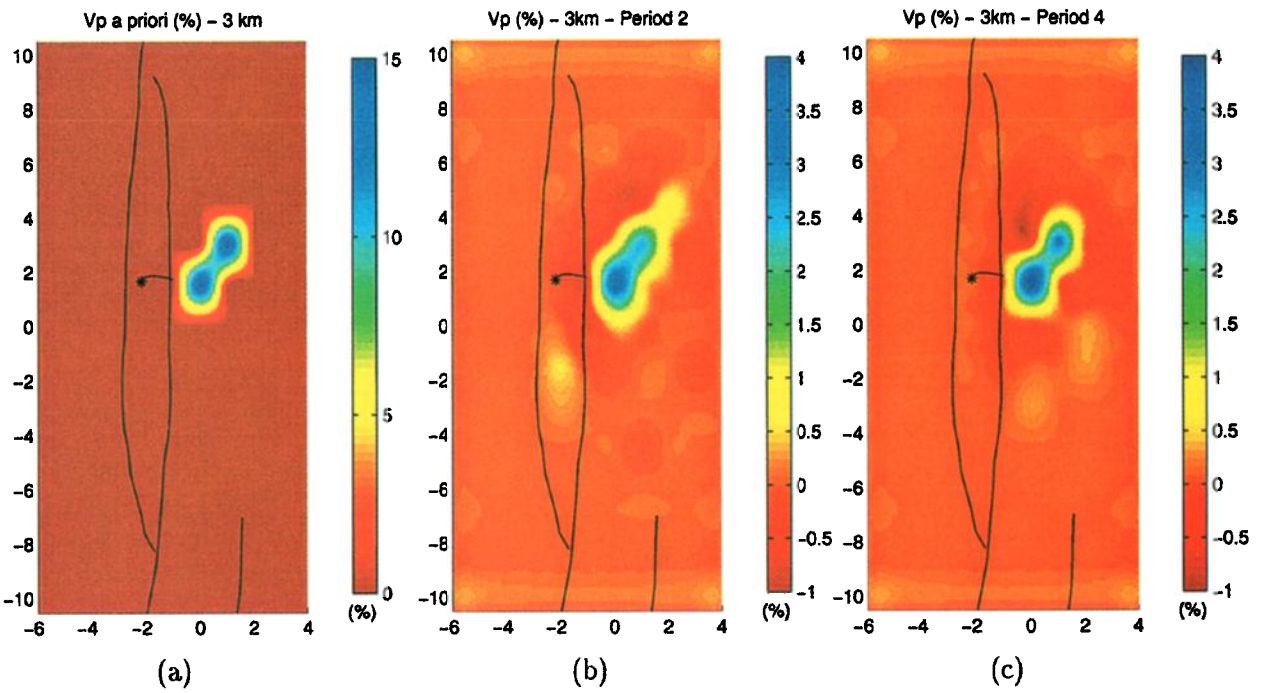


Plate 4. Test for the detected period 2 and 4 anomalies. The velocity perturbation (%) to an homogeneous velocity model (V_p) of 4 km s^{-1} is shown. (a) Two 15% velocity perturbations have been introduced in the a priori homogeneous model. This model was used for the computation of synthetic travel times for both seismicity distributions of periods 2 and 4. (b and c) Results of the P wave velocity model after the inversion of synthetic travel times are shown for periods 2 and 4 at layer node 3 km.

10°09'-11°06'N, [*Narag et al.*, 1993]). The possibility of occurrence of this event within the geothermal field has been rejected for two reasons. First, the Harvard location is biased in the direction 50-80° and 230-260° due to the lack of stations in the Indian and Pacific Oceans, so that the latitude of the expected event along the East Fault Line might be in between 11.02° and 11.03°N (i.e., south of the geothermal field). Second, geodetic measurements conducted in February 1991, June 1993, May 1994, November 1995, and June 1997 all along the West and Central Fault Lines have shown a yearly repeated shear velocity close to 2.4 cm yr^{-1} [*Duquesnoy et al.*, 1994; *Duquesnoy*, 1997; *Bacolcol*, 1999], which do not indicate any faster slip because of such an earthquake within the geothermal site.

The question which is to be discussed next concerns the possibility of establishing the seismic or aseismic behavior of these fault segments from seismic observations. Considering the cumulated shear displacement up to 15.2 cm that occurred within 76 months, it is of interest to evaluate the magnitude and seismic moment that would produce a single event for the corresponding observed displacement. For a pure uniform shear motion the seismic moment (M_0) is related to the shear modulus (G), to the area of the source (S), and to the dislocation amplitude (d) by $M_0 = GSd$. Define S as the product of the length of the fault where displacements have been measured, i.e, 15 km, by the depth of the seismogenic zone which is close to 8 km. If the shear modulus is taken as 15 GPa, the observed displacement should produce a seismic moment close to 2.74×10^{17} N m. Using *Kanamori and Anderson*'s [1975] empirical relationship between magnitude and seismic moments for major earthquakes, one might have expected an earthquake with magnitude of the order of 5.6, when none was observed. We consider next the possibility in which slip occurred in multiple seismic events; 220 events of magnitude 4 or 220,000 events of magnitude 2 would be needed to generate the expected slip motion. Also, *Pearson* [1982] has developed a similar relationship between magnitude and seismic moments for microseismic events induced by forced fluid flow with observations from The Geysers geothermal field in northern California. This relation leads to higher expected level of microseismicity. Hence it is concluded that the observed displacements are not generated seismically. This is confirmed by the lack of events observed for the period during which our dense seismic network was operated. Hence it is concluded that the fault motion is indeed aseismic and insensitive to the large water injection conducted during our experiment. These results are consistent with the fact that the continental vertical strike-slip Philippine Fault creeps at a rate of 3.5 cm yr^{-1} along its northern Leyte 50-km segment [*Duquesnoy*, 1997].

5.2. Velocity Anomaly

The injection experiment in well MG2RD and the injection programs in the six other wells have induced >400 seismic events in a volume of rock estimated at 1.75×10^8 m^3. Hence the volume of the induced seismic cloud coincides with a volume in which the pore pressure has been increased. The injection temperature was 25°C for the water used in MG2RD and close to 150°C for the hot brines injected in the other wells. The total injected volume has been estimated at 36,000 m^3 for the MG2RD injection and at 327,000 ± 20,000 m^3 for all other injections combined together.

The factors affecting seismic velocity include porosity, confining pressure, lithology, pore pressure, saturation or phase transitions, and temperature [*Nur*, 1987]. In an attemp to interpret rapid P wave velocity increase, only pore pressure, saturation, phase transitions, and temperature effects are discussed since no variation from porosity, lithology, or confining pressure are anticipated.

If the pore pressure increases in a saturated rock, so does the pore volume and this induces a correlative decrease of the P wave velocity. This effect has been clearly illustrated by *Wyllie et al.* [1958] using experimental data. So it is anticipated that the flow of liquid water within a liquid saturated body would induce a decrease in P wave velocity. Yet an increase has been detected ~1 km east of well MG2RD.

Regarding temperature effects caused by dilatation, P and S wave velocities increase when the temperature decreases, but this velocity increase remains smaller than 5% for a 100°C temperature variation according to *Bourbié et al.* [1986]. Thus the perturbation to be expected from the injection of water at 25°C (MG2RD) and brines at 160°C (others wells) should not have been larger than a few percent. On the contrary, *Fehler* [1981] described a velocity decrease with a temperature decrease, but this effect was attributed to an increase in the microcrack porosity as a result of long-term heat extraction. Given the small temperature variation anticipated from the injections, this mechanism is not considered here.

At The Geysers geothermal fields in California, low-velocity ratios were interpreted as low pore pressure and dry conditions, caused by the boiling of water as steam was extracted [*Julian et al.*, 1996]. It is proposed here that the observed increase in velocity, in Tongonan, is linked with the invasion of liquid water in a nonliquid saturated rock body, i.e., within a pore volume partially filled with vapor or gas. Some laboratory measurements [*Domenico*, 1976] have pointed out nonlinear variations of P wave velocity with saturation. This phenomenon of imbibition (displacement of gas by water), predicted by

the Biot-Gassmann-Domenico theory [*Domenico*, 1976], shows that V_p drastically increases (~30%) when saturation is within a range of 80% to 100%. First, V_p gradually decreases with increasing saturation because of the effective density increase, but when the full saturation is nearly reached, V_p drastically increases because the pore fluid compressibility effect outweighs the density effect. More recently, *Le Ravalec and Guéguen* [1996] have modeled this effect as the result of two scale heterogeneities, one related to the size of pores and cracks, the other one to the size of the heterogeneities of the fluid phase distribution.

The argument for considering nonsaturated conditions, in this area of the geothermal reservoir, is threefold.

First, thermodynamical conditions in the reservoir have been examined in order to ascertain the possibility of having pore volume partially filled with liquid and vapor. For example, borehole MG21D exibits temperature and pressure values equal to 290°C and 7.4 MPa, respectively, at depth 1000 m bgs. This corresponds to the vapor-liquid water transition (Table 2) [*Lide*, 1992]. Unsaturated conditions can also be observed in the reservoir where temperature reaches 320°C at ~1000 m bgs. Moreover, the temperature profile in MG21D is characteristic of a convection process and indicates that higher temperature exists in the vicinity of the well. Hence we expect temperatures higher than 300°C that would explain nonsaturated conditions at depths >1000 m bgs. When we try to evaluate the weight of a water column given a density gradient related to the temperature gradient on site, the results indicate that liquid pressure is close to 14 MPa for a temperature of 340°C at 2000 m bgs, it still corresponds to partially saturated conditions. This evaluation seems realistic since pore pressure will not increase drastically if pore volume contains vapor.

Second, it has already been mentioned that the injectivity index has been strongly reduced for well MN3RD 2 months after period 4 and slighty for wells MN2RD and MG21D. This may be related to the fact that saturation occurs in these wells and that maximum capacity for injection is reached rapidly.

Third, let us assume that the perturbed volume of rock was initially unsaturated with a saturation within a range of 80% to 100% to allow a nonlinear P wave velocity increase. In that case, the initial conditions must be close to full saturation, so that a small amount of liquid would saturate the pore volume and would allow the observed increase in pore pressure. We consider an initial saturation equal to 95%. If we estimate the volume of rock perturbed by the invasion of the injected liquid (porosity of 6%), this would yield a volume equal to 1.34×10^8 m^3. This computed volume is smaller than the volume of rock in which induced seismicity has been observed but has the same order of magnitude. It means that most of the induced seismicity occurred in a volume where the increase in pore pressure is allowed only after some vapor has been replaced by some liquid water.

Table 2. Vapor Pressure-Temperature Conditions of Water [Lide, 1992]

T, °C	P, MPa
260	3.34
280	6.41
300	8.58
320	11.28
340	14.59
360	18.6
373	21.8

Hence we propose the following mechanism to interpret the observation. Before injection, a nonsaturated medium prevailed with a pore volume (V_p) partially filled with a liquid volume (V_l) and a gas vapor volume (V_g) and with a pore pressure P_p. The saturation was close to 100%. After the beginning of the injections (injected volume V_j), invasion and slight cooling occurred, leading to a reduction of the volume of vapor followed by a phase change (constant P_p, $V_p = V_l + V_j + V_{g\to l}$, $V_{g\to l}$ is the volume of liquid due to the phase change). When saturation was fully reached, pore pressure increased, and a small amount of liquid volume (ΔV_{lS}) was absorbed by the compressibility of the liquid ($V_p = V_l + V_j + V_{g\to l} - \Delta V_{lS}$). The main contribution of this volume effect is provided by the invasion phenomenon. This evaluation is consistent with the order of magnitude that would induce a significant perturbation to the observed travel times. Because the injected water is distributed nonuniformly close to each well and the saturation and porosity will be heterogeneous, we suggest that the perturbed volume may be even larger than that which has been computed.

Accordingly, it seems reasonable to interpret the observed P wave velocity increase as induced by a decrease in vapor content. In Tongonan this suggests that tomographic inversion of velocity could provide valuable informations for identifying geothermal resources and for monitoring them during exploitation.

6. Conclusions

A large water injection has been undertaken in a well that intersects a creeping segment of the Philippine Fault, at the Tongonan geothermal field. Various other injection programs were conducted simultaneously in the vicinity of the well with larger injected volumes but lower wellhead pressures. The MG2RD experiment has shown that most of the water was injected to the east of the Central Fault Line.

More than 400 events were recorded in the vicinity of the well and have been located through a simultaneous 3-D velocity-hypocenter inversion procedure. None of the induced microeathquakes is located along the creep-

ing Central Fault Line, and all of them occurred below the casing shoe to the east of the fault line, i.e., within the geothermal reservoir. The increase in wellhead pressure with associated microseismicity strongly suggests that pore pressure is the mechanism responsible for the observed induced seismicity for the injection experiment.

The absence of induced events along the Central Fault Line, combined with the lack of microseismicity along the two central and west branches of the fault over a broad range of time, indicate an aseismic behavior of the fault at this location. These results have to be considered with the fact that the continental vertical strike-slip Philippine Fault creeps at a rate of 3.5 cm yr^{-1} along its northern Leyte 50-km segment.

The 3-D velocity model imaged during injections, compared to that obtained from seismic monitoring conducted prior to the injection experiment, shows a localized significant increase of P wave velocity. This anomaly is within the seismicity cloud associated with the water injection. This effect is interpreted as being the results of an increase in liquid content within a liquid-vapor multiphase part of the reservoir. These observations may reveal significant for constraining the pore pressure in the vicinity of the fault.

Acknowledgments. The hydraulic stimulation was supported by PNOC (Philippine National Oil Company) and a grant from the Philippino Department of Sciences and Technology, which was obtained thanks to R. Punongbayan and E. Ramos (PHIVOLCS). All the seismic work has been supported by the French Ministry of Foreign Affairs and by PHIVOLCS within the framework of the French-Philippino cooperation. This project was initiated by R. Gaulon (IPGP) and E. Barrier (UPMC) and benefitted from the support of H. Ferrer (PNOC). Most of the seismic instruments were provided by EOPGS. Special thanks are due to J. Sahr (EOPGS) for the emergency repairs of instruments struck by lightning and for efficient handling of the telemetred network. We would like also to thank E. Caballes (PNOC), D. Martinez (PHIVOLCS), S. Luther (PHIVOLCS) and F. Maneja (PNOC) for participating in the data gathering and maintenance of the instruments. We also thank M. Frogneux (EOPGS) and A. Nercessian (IPGP) for their help and experience in the preparation of a clean database and for initial data processing. This work benefitted from fruitful discussions with T. Mossop. This is also IPGP contribution 1672.

References

Allen, C.R., Circum-Pacific faulting in the Philippines-Taiwan region, *J. Geophys. Res.*, *67*, 4,795-4,811, 1962.

Aurelio, M., Tectonique du segment central de la Faille Philippine, Etude structurale, cinématique et évolution géodynamique, thèse de doctorat, Univ. Paris 6, Paris, 1992.

Bacolcol, T. C., Etude d'un segment de la Faille Philippine à partir de données GPS, stage de DEA, Univ. Paris 6, Paris, 1999.

Barrier, E., M. Aurelio, C. Muller, M. Pubellier, R. Quebral, and C. Rangin, La Faille Philippine : Un exemple de grand décrochement actif à l'arrière d'une zone de subduction, *C. R. Acad. Sci. Ser. II*, *311*, 181-188, 1990.

Barrier, E., P. Huchon, and M. Aurelio, Philippine Fault: A key to Philippine kinematics, *Geology*, *19*, 32-35, 1991.

Bondocoy, D., MG2RD completion test report, technical report, PNOC - Energy Dev. Corp., Makati City, Philippines, 1993.

Bourbié, T., O. Coussy, and B. Zinszner, *Acoustique des Milieux Poreux*, Technip, Paris, 1986.

Cornet, F.H., Fracture processes induced by forced fluid percolation, *Volcanic Seismology, IAVCEI Proceedings in Volcanology*, Vol. 3, edited by P., Gasparini, R., Scarpa and K. Aki, pp. 407-431, Springer-Verlag, New York, 1992.

Cornet, F.H., and R. Jones, Field evidence on the orientation of forced water flow with respect to the regional principal stress directions, *Rock Mechanics-Models and Measurements*, edited by P.P., Nelson and S.E., Laubach, pp. 61-71, A.A. Balkema, Brookfield, VT., 1994.

Cornet, F.H., J. Helm, H. Poitrenaud, and A., Etchecopar, Seismic and aseismic slips induced by large scale fluid injections, *Pure Appl. Geophys.*, *150*, 563-583, 1997.

Delfin, F. Jr., F. Maneja, D. Layugan, and M. Zaide-Delfin, Stratigraphic and geophysical constraints on injection targets in the greater Tongonan geothermal field, Leyte, Philippines, technical report, PNOC - Energy Dev. Corp., Makati City, Philippines, 1995.

Domenico, S., Effect of brine-gas mixture on velocity in an unconsolidated sand reservoir, *Geophysics*, *41*, 882-894, 1976.

Dorbath, C., D. Oppenheimer, F. Amelung, and G. King, Seismic tomography and deformation modeling of the junction of the San Andreas and Calaveras faults, *J. Geophys. Res.*, *101*, 27,917-27,941, 1996.

Duquesnoy, T., Contribution de la géodésie à l'étude de grands décrochements actifs associés à des zones de subduction à convergence oblique, thèse de doctorat, Univ. Paris-Sud, Orsay, France, 1997.

Duquesnoy, T., E. Barrier, M. Kasser, M. Aurelio, R. Gaulon, R. Punongbayan, C. Rangin, and the French-Philippine Cooperation Team, Detection of creep along the Philippine Fault: First result of geodetic measurements on Leyte island, central Philippines, *Geophys. Res. Lett.*, *21*, 975-978, 1994.

Eberhart-Phillips, D., Three-dimensional velocity structure in northern California Coast Ranges from inversion of local earthquake arrival times, *Bull. Seismol. Soc. Am.*, *76*, 1,025-1,052, 1986.

Eberhart-Phillips, D., Three-dimensional P and S velocity structure in the Coalinga region, California, *J. Geophys. Res.*, *95*, 15,343-15,363, 1990.

Eberhart-Phillips, D., Local earthquake tomography: Earthquake source regions, *Seismic Tomography: Theory and Practice*, edited by H.M., Iyer, and K., Hirahara, pp. 613-643, Chapman and Hall, New York, 1993.

Evans, J., D. Eberhart-Phillips, and C. Thurber, User's manual for SIMULPS12 for imaging V_p and V_p/V_s, a derivative of the Thurber tomographic inversion SIMUL3 for local earthquakes and explosions, *U.S. Geol.Surv. Open File Rep.*, *94-431*, 142 pp., 1994.

Evans, J.R., and U. Achauer, Teleseismic velocity tomography using the ACH method: Theory and application to continental-scale studies, *Seismic Tomography: Theory and Practice*, edited by H.M., Iyer, and K., Hirahara, pp. 319-360, Chapman and Hall, New York, 1993.

Fehler, M., Changes in P wave velocity during operation of a hot dry rock geothermal system, *J. Geophys. Res.*, *86*, 2,925-2,928, 1981.

Fehler, M., Stress control of seismicity patterns observed during hydraulic fracturing experiments at the Fenton Hill

hot dry rock geothermal energy site, New Mexico, *Int. J. Rock Mech. Min. Sci.*, *26*, 211-221, 1989.

Fitch, T., Plate convergence, transcurrent faults, and internal deformation adjacent to SE Asia and the western Pacific, *J. Geophys. Res.*, *77*, 4,432-4,460, 1972.

Foulger, G., and A. Miller, Three-dimensional V_p and V_p/V_s structure of the Hengill Triple Junction and geothermal area, Iceland, and the repeatability of tomographic inversion, *Geophys. Res. Lett.*, *22*, 1,309-1,312, 1995.

Julian, B., A., Ross, G. Foulger, and J. Evans, Three-dimensional seismic image of a geothermal reservoir: The Geysers, California, *Geophys. Res. Lett.*, *23*, 685-688, 1996.

Kanamori, H., and D. L. Anderson, Theoretical basis of some empirical relations in Seismology, *Bull. Seismol. Soc. Am.*, *65*, 1073-1095, 1975.

Kissling, E., W. Ellsworth, D. Eberhart-Phillips, and U. Kradolfer, Initial reference models in local earthquake tomography, *J. Geophys. Res.*, *99*, 19,635-19,646, 1994.

Klein, F., User's guide to HYPOINVERSE, a program for vax computers to solve for earthquake locations and magnitude, *U.S. Geol. Surv. Open File Rep.*, *89-314*, 49 pp., 1989.

Le Ravalec, M., and Y. Guéguen, Elastic wave velocities in partially saturated rocks: Saturation hysteresis, *J. Geophys. Res.*, *101*, 837-844, 1996.

Lide, D., *Handbook of Chemistry and Physics*, 73rd ed., CRC Press, Boca Raton, Fla., 1992.

Mossop, A., Seismicity at The Geysers geothermal field: Correlations and mechanisms, *Eos Trans., AGU*, *79* (17), Spring Meet. Suppl., S227, 1998.

Narag, I., B. Marte, and A. Valerio, May 17, 1993 Tongonan Leyte earthquakes-Preliminary Report of Investigation, technical report, PHIVOLCS, Quezon City, Philippines, 1993.

Nur, A., Seismic rock properties for reservoir descriptions and monitoring, *Seismic Tomography-With Applications in Global Seismology and Exploration Geophysics*, edited by G. Nolet, pp. 203-237, D. Reidel, Norwell, Mass., 1987.

Pearson, C., The relationship between microseismicity and high pore pressures during hydraulic stimulation experiments in low permeability granitic rocks, *J. Geophys. Res.*, *86*, 7,855-7,864, 1981.

Pearson, C., Parameters and a magnitude moment relationship from small earthquakes observed during hydraulic fracturing experiments in cristalline rocks, *Geophys. Res. Lett.*, *9*, 404-407, 1982.

Pine, R. and A. Batchelor, Downward migration of shearing in jointed rock during hydraulic injections, *Int. J. Rock Mech. Min. Sci.*, *21*, 149-263, 1984.

Segall, P., Earthquakes triggered by fluid extraction, *Geology*, *17*, 942-946, 1989.

Thurber, C., Earthquake locations and three-dimensional crustal structure in the Coyote Lake area, central California, *J. Geophys. Res.*, *88*, 8,226-8,236, 1983.

Thurber, C., Local earthquake tomography: Velocities and V_p/V_s theory, *Seismic Tomography: Theory and Practice*, edited by H.M. Iyer, and K., Hirahara, pp. 563-583, Chapman and Hall, New York, 1993.

Wyllie, M., A. Gregory, and G. Gardner, An experimental investigation of factors affecting elastic wave velocities in porous media, *Geophysics*, *23*, 459-493, 1958.

F.H. Cornet and R. Prioul, Dépt. de Sismologie, Institut de Physique du Globe de Paris, 4 place Jussieu, F-75252 Cedex 05 Paris, France (cornet@ipgp.jussieu.fr; prioul@ipgp.jussieu.fr).

C. Dorbath and L. Dorbath, Dépt. de Sismologie, Institut de Physique du Globe de Strasbourg, 5 rue René Descartes, F-67084 Strasbourg cedex, France (cath@sismo.u-strasbg.fr; louis@sismo.u-strasbg.fr).

M. Ogena, Geoscientific Division, Philippine National Oil Compagny, Energy Development Corporation, Fort Bonifacio, Makati City, Philippines (ogena@edc.energy.com.ph).

E. Ramos, Philippine Institute of Volcanology and Seismology, C.P. Garcia Avenue, U.P. Diliman, Quezon City, Philippines (eramos@phivolcs.dost.gov.ph).

(Received July 12, 1999; revised January 26, 2000; accepted February 9, 2000.)